The EMBO Journal Vol. 21 No. 22 pp. 5969–5978, 2002

Microscopic evidence for a minus-end-directed power stroke in the kinesin motor ncd

Thomas G.Wendt, Niels Volkmann[1], Georgios Skiniotis, Kenneth N.Goldie, Jens Müller[2], Eckhard Mandelkow[2] and Andreas Hoenger[3]

European Molecular Biology Laboratory, Structure Programme, Meyerhofstrasse 1, D-69117 Heidelberg, [2]Max Planck Unit for Structural Biology, DESY, Notkestrasse 85, D-22607 Hamburg, Germany and [1]The Burnham Institute, North Torrey Pines Road, La Jolla, CA 92037, USA

[3]Corresponding author
e-mail: hoenger@embl-heidelberg.de

We used cryo-electron microscopy and image reconstruction to investigate the structure and microtubule-binding configurations of dimeric non-claret disjunctional (ncd) motor domains under various nucleotide conditions, and applied molecular docking using ncd's dimeric X-ray structure to generate a mechanistic model for force transduction. To visualize the α-helical coiled-coil neck better, we engineered an SH3 domain to the N-terminal end of our ncd construct (296–700). Ncd exhibits strikingly different nucleotide-dependent three-dimensional conformations and microtubule-binding patterns from those of conventional kinesin. In the absence of nucleotide, the neck adapts a configuration close to that found in the X-ray structure with stable interactions between the neck and motor core domain. Minus-end-directed movement is based mainly on two key events: (i) the stable neck–core interactions in ncd generate a binding geometry between motor and microtubule which places the motor ahead of its cargo in the minus-end direction; and (ii) after the uptake of ATP, the two heads rearrange their position relative to each other in a way that promotes a swing of the neck in the minus-end direction.

Keywords: cryo-electron microscopy/helical 3-D image reconstruction/kinesin/microtubule/ncd

Introduction

Kinesin-like motors are key components in microtubule (MT)-based motility systems. Cellular, biochemical and structural studies of the kinesin superfamily revealed a rather detailed picture of their functions and properties. The most common architecture of kinesin family members is a dimeric structure which features three distinct domains: (i) a conserved motor domain that contains the ATP-dependent MT-binding site; (ii) a central α-helical stalk region responsible for dimerization; and (iii) a tail domain that is involved in cargo binding and regulation of motor-specific functions (for recent reviews, see Bloom and Goldstein, 1998; Hirokawa, 1998; Mandelkow and Johnson, 1998; Sheetz, 1999). Apart from dimeric kinesins, monomeric, tetrameric and heterotrimeric forms have also been described (Hirokawa, 1998). The interaction of kinesin-like motor domains with MTs has been studied extensively by electron microscopy (EM) and computational three-dimensional analysis (for reviews, see Mandelkow and Hoenger, 1999; Vale and Milligan, 2000). The near-atomic resolution three-dimensional map of the αβ-tubulin heterodimer (Nogales *et al*., 1998) allowed interpretation in atomic detail of the intermediate resolution cryo-EM structures of MTs (Nogales *et al*., 1999) and of kinesin motor–MT complexes (Hoenger *et al*., 2000; Kikkawa *et al*., 2001).

The *Drosophila* motor non-claret disjunctional (ncd; McDonald *et al*., 1990; Walker *et al*., 1990) is involved in spindle assembly and maintenance during meiosis and early mitosis. Its structure has been solved to atomic resolution by X-ray crystallography (Sablin *et al*., 1996, 1998). Ncd is composed of three distinct domains: a conserved motor domain located at the C-terminal end of the polypeptide chain (residues 356–700); a central stalk region (residues 200–356); and an N-terminal tail domain (residues 1–200) involved in cargo binding. The tail domain of ncd contains a second, ATP-independent, MT-binding domain (McDonald *et al*., 1990; Chandra *et al*., 1993). Despite the structural similarities between the ncd and kinesin core motor domains, they exhibit significantly different behavior: kinesin is a fast and highly processive anterograde motor, whereas ncd is a non-processive retrograde motor (McDonald and Goldstein, 1990; Walker *et al*., 1990; deCastro *et al*., 1999; Pechatnikova and Taylor, 1999; Foster and Gilbert, 2000).

Previous cryo-EM and three-dimensional reconstructions by several groups revealed a good consensus view of the structure of monomeric or dimeric ncd motor domains complexed with MTs in the presence of AMP-PNP (Hirose *et al*., 1996, 1998; Sosa *et al*., 1997). Ncd monomers formed a tight 1:1 complex with β-tubulin subunits on the MT surface so that each αβ-tubulin heterodimer was decorated with one motor domain (Hoenger and Milligan, 1997). Ncd dimers adopted a 'one-headed' binding state, where only one motor head was bound to β-tubulin (here named 'head 1' throughout the text, and colored in yellow in all figures), whereas the second head (head 2; red) was loosely tethered to the first, projecting away from the MT surface (Hirose *et al*., 1996; Sosa *et al*., 1997). Here we could confirm this asymmetric binding conformation for two strong binding states, one in the absence of nucleotide and the other in the presence of AMP-PNP, mimicking an ATP state. Ncd in the presence of excess ADP binds to MTs only very weakly. Since the density of the α-helical coiled-coil neck is too low to be observed directly with the methods applied here, we engineered an SH3 domain N-terminal to residue 296 of the ncd construct as an

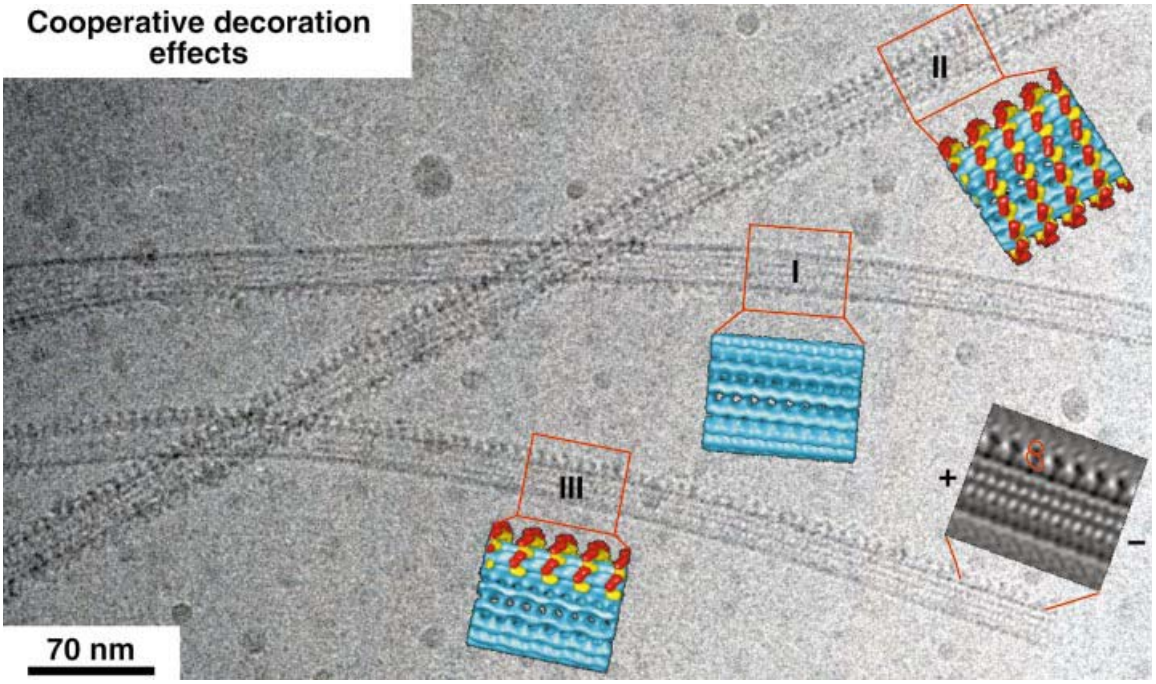

Fig. 1. A cryo-EM image of MTs decorated with dimeric ncd at subsaturating ratios reveals a cooperative binding mechanism in the axial direction, along individual protofilaments. While one of the MTs is mostly undecorated (I), partial decoration (III) and complete decoration (II) co-exist in the same area. A Fourier-filtered image of the MT and the motors in a side projection allows determination of the polarity of the MT according to the shape of the dimeric motor construct.

additional density marker. We could localize the position of the neck in a nucleotide-free state. In the presence of AMP-PNP, however, the neck could not be visualized, probably due to an increased flexibility within this region.

We interpreted our cryo-EM-based three-dimensional data with the help of the dimeric ncd crystal structure (Sablin *et al*., 1998) to generate a mechanistic model for minus-end-directed force transduction in ncd. The ncd crystal structure contains ADP in both nucleotide pockets and shows distinct contacts between the head domains (helix α1, and loops 6, 10 and 13) and the corresponding neck helix (Sablin *et al*., 1998). We found these contacts to be maintained in the absence of nucleotides, but disrupted, at least for the head that binds to tubulin in the presence of AMP-PNP. This conformational change forces the neck into a new position towards the MT minus end. The structural evidence presented here suggests a force-transducing mechanism in ncd, which is clearly different from conventional kinesin. In some functional (but not mechanistic) aspects, it resembles the action of myosin II (see, for example, Geeves and Holmes, 1999), in particular the lack of processive motion (Foster and Gilbert, 2000) and the requirement for several motors to produce effective movement (deCastro *et al*., 1999). These observations, combined with data from other groups (Pechatnikova and Taylor, 1999; deCastro *et al*., 2000; Foster *et al*., 2001) may explain how ncd generates a minus-end-directed motion in a non-processive fashion. While inefficient for processive long-distance travel (e.g. in axonal transport), the mechanism proposed here is perfectly suited for a task such as the organization and bundling of MTs into spindles by multiple ncd motors operating together in a complex assembly.

Results

Dimeric ncd head domains bind to microtubules in a cooperative fashion

In a first set of experiments, we decorated MTs with dimeric ncd head domains at under-saturating conditions (i.e. 2-fold fewer heads than available binding sites) at a motor:tubulin ratio of 0.21:0.5 mg/ml to study the binding patterns, cooperative effects and the influence on MT stabilization by motors. Ncd dimers decorate MTs in a highly cooperative fashion (Figure 1). This is particularly obvious in the absence of nucleotide, but to a lesser extent also in the presence of AMP-PNP. As shown in Figure 1, empty MTs can be found next to fully decorated ones and, even more strikingly, we found many MTs that show a complete decoration of only one or two protofilaments (Figure 1, III). This indicates that cooperative decoration proceeds mostly in the axial direction (compare with Vilfan *et al*., 2001). Based on the Fourier filtering, we determined the polarity of the partially decorated MT by comparing the projected shape of the head domains with that of three-dimensional reconstructions. Accordingly, its minus end is to the right.

The strong microtubule-binding states reveal an asymmetric configuration with different MT affinities in the two heads

Strong binding of ncd to MTs occurs in two distinct states: in the absence of nucleotides (after apyrase treatment of all solutions) and in the presence of AMP-PNP, which mimics an ATP-bound state. Under both conditions, ncd binds asymmetrically, which means one head binds to tubulin (here called head 1; yellow in all figures) and the other

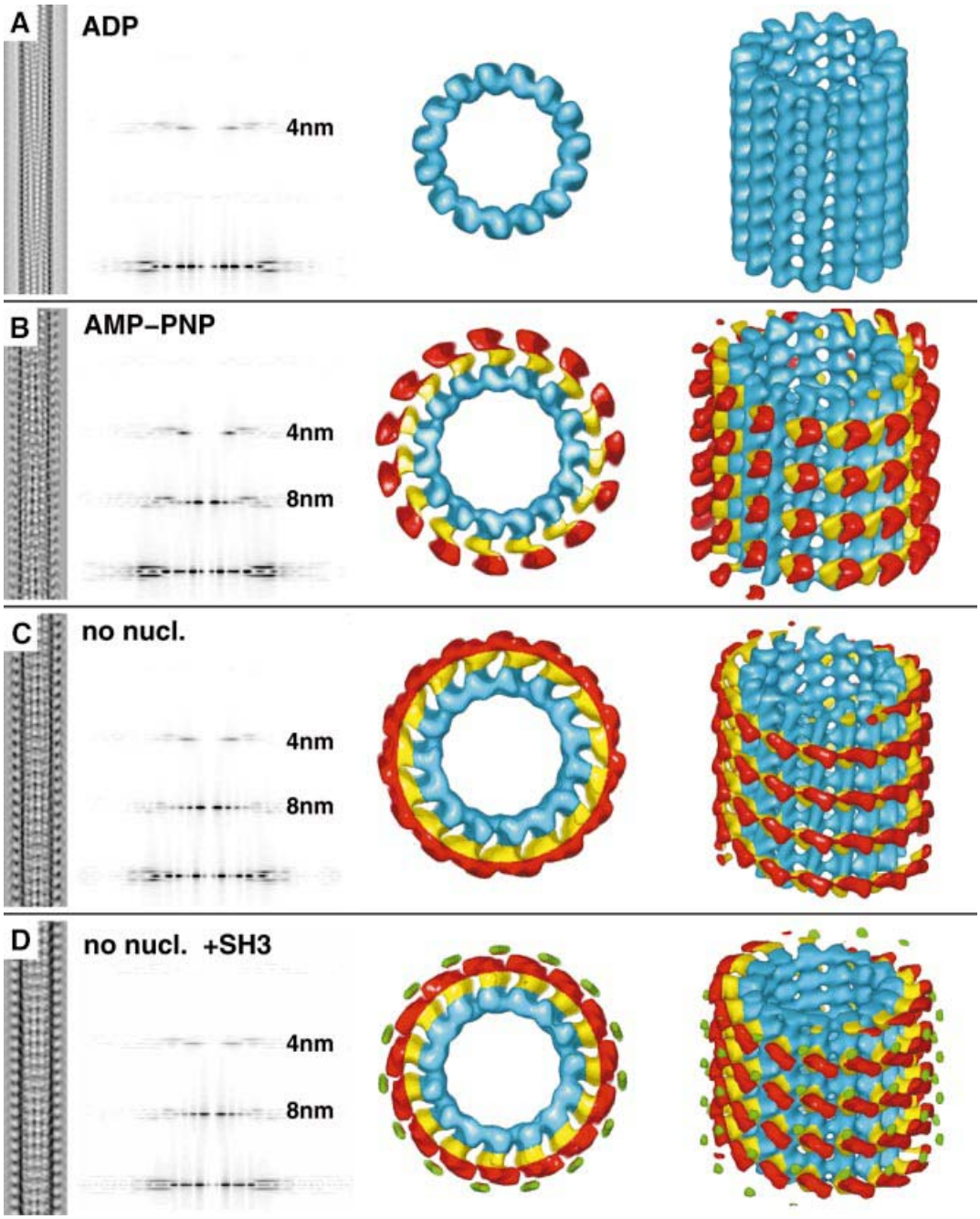

Fig. 2. Helical three-dimensional reconstructions of MTs decorated with dimeric ncd head domains under various nucleotide conditions. Left columns show the projected three-dimensional reconstructions of each condition, with the corresponding diffraction patterns in the second column from the left. Surface-rendered three-dimensional constructions are shown in the two columns on the right. (**A**) No significant decoration is achieved in the presence of excess ADP. (**B**) Dimeric ncd in the presence of AMP-PNP binds to tubulin with one of its heads (head 1) while the second head (head 2) locates on top of the bound one. (**C**) Absence of nucleotides creates a state similar to that in (B), but with head 2 rotated by ~90°. (**D**) Only in the absence of nucleotide was it possible to detect a significant density coming from an SH3 domain (green volumes), which we engineered at the N-terminus of our construct to increase its visibility. This density was absent in reconstructions from tubes decorated with ncd in the presence of AMP-PNP, indicating an increased flexibility in the neck region.

remains unbound (here called head 2; red in all figures) in a configuration on top of the bound head (Figure 2; see also Hirose *et al*., 1996; Sosa *et al*., 1997). Nevertheless, the two conformational states of dimeric ncd bound to MTs are clearly different from each other, and are strikingly different from those found for conventional kinesin where both heads bind simultaneously to the MT surface (Hoenger *et al*., 2000). As shown in Figure 2B and C, the AMP-PNP state is slightly more upright than the no-nucleotide state. While head 1 (yellow) appears to assume an identical configuration in both states, head 2 undergoes a substantial rotation which directs the neck towards the minus end of the MT (Figures 3 and 4). Details of the cryo-EM three-dimensional reconstructions are summarized in Table I.

To enhance the visibility of the neck in cryo-EM preparations, and to monitor its movements during the ATP hydrolysis cycle, we engineered an SH3 domain as a

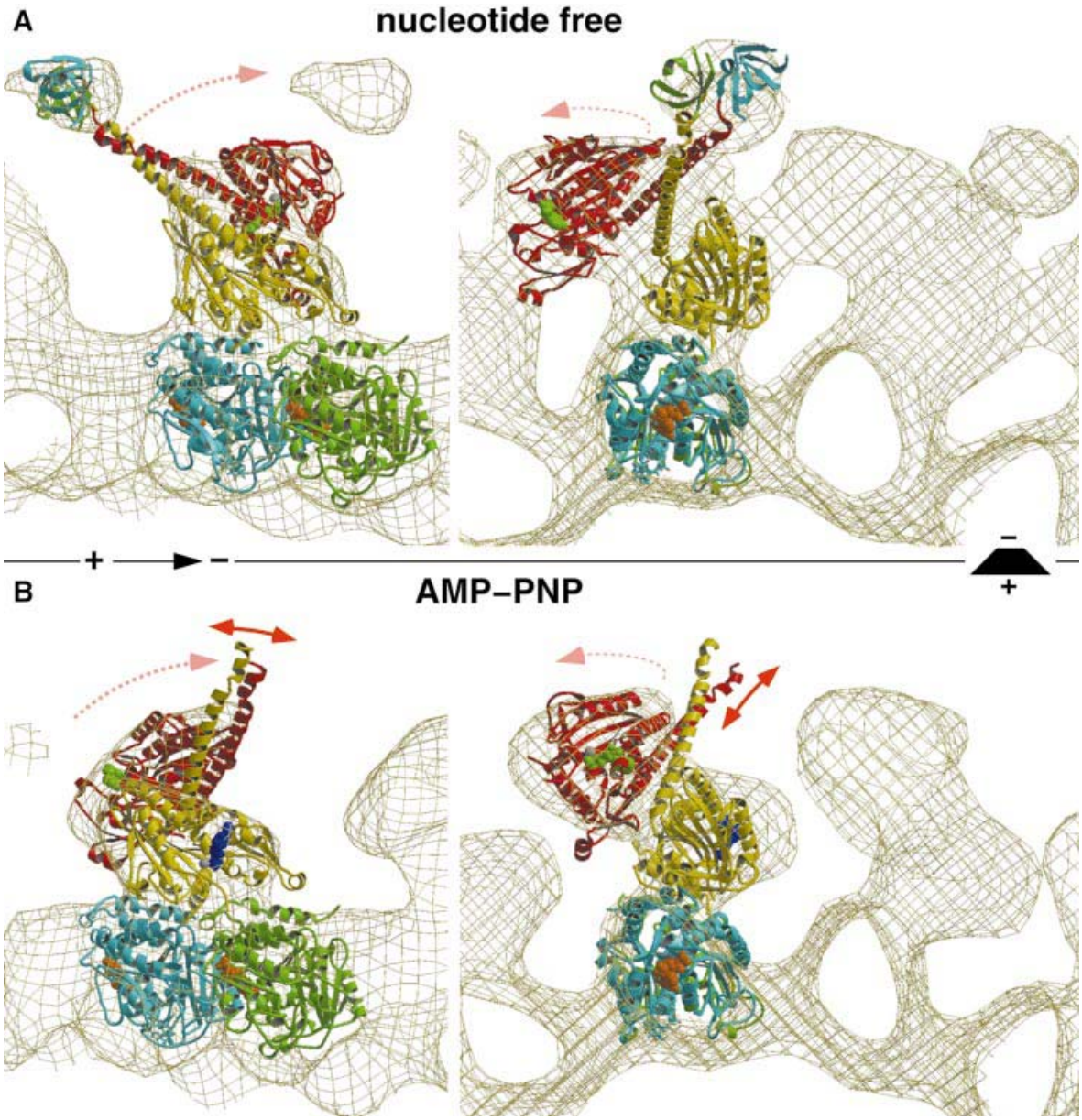

Fig. 3. Molecular docking and modeling, fitting the atomic resolution X-ray structure from Sablin *et al.* (1998) into our EM-derived three-dimensional maps of MT–ncd complexes. The panels on the left show side views of a protofilament with the plus end to the left. The right panels show end-on views of protofilaments viewed from the plus end. (**A**) The conformation of dimeric ncd in the absence of nucleotides strongly resembles the ADP state found in the crystal structure. The neck was visualized by two SH3 domains engineered to the N-terminal ends of the neck helices. (**B**) The neck of the untagged construct was not visible in the presence of AMP-PNP due to an increased flexibility in that region. Nevertheless, our docking experiments revealed a large conformational change, rearranging heads 1 and 2 dramatically. Head 2 rotates around a radial axis located at the C-terminal end of the neck (the transition into the core). Thereby, the two heads approach each other and close the gap towards the plus end, thus moving the neck into the minus-end direction.

density marker on the N-terminus of the neck helix in the construct (G.Skiniotis, T.Surrey, S.Altmann, H.Gron, Y.-H.Song, E.Mandelkow and A.Hoenger, submitted). This SH3–ncd construct will be called tagged ncd in the following. The density from two neighboring globular SH3 domains at the end of the dimeric neck coiled-coil adds up to ~14 kDa and can be detected in configurations where the neck is stabilized between the two heads. The SH3 domains were clearly visible in the absence of nucleotides (Figure 2D, green densities) pointing towards the MT plus end (see docking in Figure 3A) in a similar configuration to that predicted by Sablin (2000). However, in the presence of AMP-PNP, the SH3 domains could not be detected, indicating an increased flexibility in this region after ATP uptake in head 1 (Figure 2B).

ADP-bound ncd exhibits a low affinity for microtubules

In the presence of ADP, no significant complex formation between the untagged ncd and MTs could be detected with our methods (Figure 2A). We took particular care to avoid inorganic phosphate, which has been reported to lower the ncd binding affinity dramatically (Foster *et al.*, 1998). We calculated a three-dimensional map from 16 combined

Table I. Statistics of three-dimensional reconstruction data

	Motor concentration (mg/ml)	Motor concentration (μM) heads	No. of asymmetric units	Average phase residual
Ncd AMP-PNP	3.3	41	~54 000	19.0
Ncd ADP	3.3	41	~35 000	18.0
Ncd no-nucleotide	4.5/2.0	55/25	~59 000	22.0
SH3–ncd no-nucleotide	4.4	42	~44 000	19.1

The MT concentration was kept constant at 0.5 mg/ml, which corresponds to 5 μM αβ-tubulin dimers. Differing amounts of motor constructs were used in the experiments (columns 2 and 3). The number of asymmetric units (column 4) and the average phase residual in the final maps (column 5) are also shown.

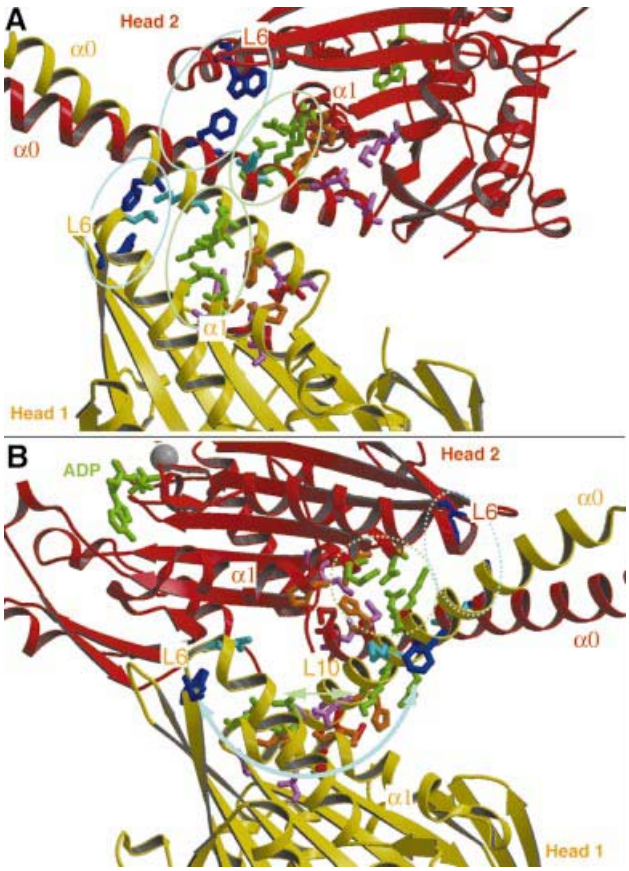

Fig. 4. The X-ray structure of dimeric ncd motor domains revealed a number of interactions between the motor cores (α1, loops 6, 10 and 13) and their corresponding neck helices (α0). (**A**) In our model, based on the docking shown in Figure 3, these interactions remain conserved for both heads in ncd dimers bound to MTs in the absence of nucleotide. (**B**) However, in the presence of AMP-PNP, these contacts may be only conserved for head 2, but not for head 1. Potential contacts now appear between loops 6 and 10 in head 1, and loop 2, β1a/b and the beginning of α1 in head 2. This indicates that ATP uptake triggers a conformational change within the motor core domain, which directly influences the neck–core interaction, and which may therefore constitute the underlying mechanism for ncd function.

data sets chosen from a large number of micrographs. This map, however, revealed basically an empty MT, with no significant mass whatsoever related to motors. By using a phosphate assay that detects inorganic phosphate at nanomolar amounts (Lanzetta *et al*., 1979), we made sure that the content of free phosphate was low enough not to influence the binding behavior of the motor. We used Sigma HPLC-purified ADP at a concentration of 2 mM that had <1% free phosphate. However, even at high stoichiometric ratios, the MTs appeared undecorated and did not show any of the characteristic spikes, in contrast to the experiments published by Hirose *et al*. (1998).

In nucleotide-free conditions, the coiled-coil neck points towards the plus end

To gain insight into the force-transducing mechanism of ncd, we interpreted the conformations found in our cryo-EM-derived three-dimensional maps with the X-ray crystal structure of dimeric ncd (Sablin *et al*., 1998). We applied quantitative molecular docking, using the program suite COAN (Volkmann and Hanein, 1999), described in Materials and methods. During the ATP hydrolysis cycle of ncd motors (see Foster *et al*., 2001), dimeric ncd in solution has ADP bound in both nucleotide pockets and binds to MTs by releasing ADP from the MT-bound head (head 1). According to Foster *et al*. (2001), head 2 keeps ADP bound during the entire hydrolysis cycle of head 1. This is the configuration that we reconstructed as the nucleotide-free state (Figures 3A and 4A). Using the SH3–ncd chimera allowed us to determine unambiguously the orientation of the two heads and the orientation of the neck coiled-coil (Figure 3A). Our molecular docking suggests that the nucleotide-free binding state remains very close to the configuration found by X-ray crystallography. As shown by Sablin *et al*. (1998), in an ADP-bound state the neck helices (marked as α0 in Figure 4) interact with their corresponding head domains (helix α1, and loops 6, 10 and 13; Figure 4A), thereby forming a very stable 2-fold symmetric complex. Our data indicate that the binding to the MT surface and the release of ADP from one of the head domains (head 1) conserves these contacts and, consequently, the dimeric ncd complex remains more or less unchanged. Accordingly, the nucleotide-free state orients the neck coiled-coil towards the MT plus end in a well-defined position (see the location of the SH3 markers in Figure 3A; see also Sablin, 2000).

Uptake of ATP into the nucleotide pocket of the microtubule-bound head induces a repositioning of the neck in the minus-end direction

The presence of excess AMP-PNP changes the ncd dimer configuration dramatically (Figures 3B and 4B). The MT-bound head appears to remain in the same orientation, but the unbound head 2 rotates by ~90° around a radial axis roughly at the C-terminal end of α1 (the transition of the neck into the core). It moves closer to head 1, thereby

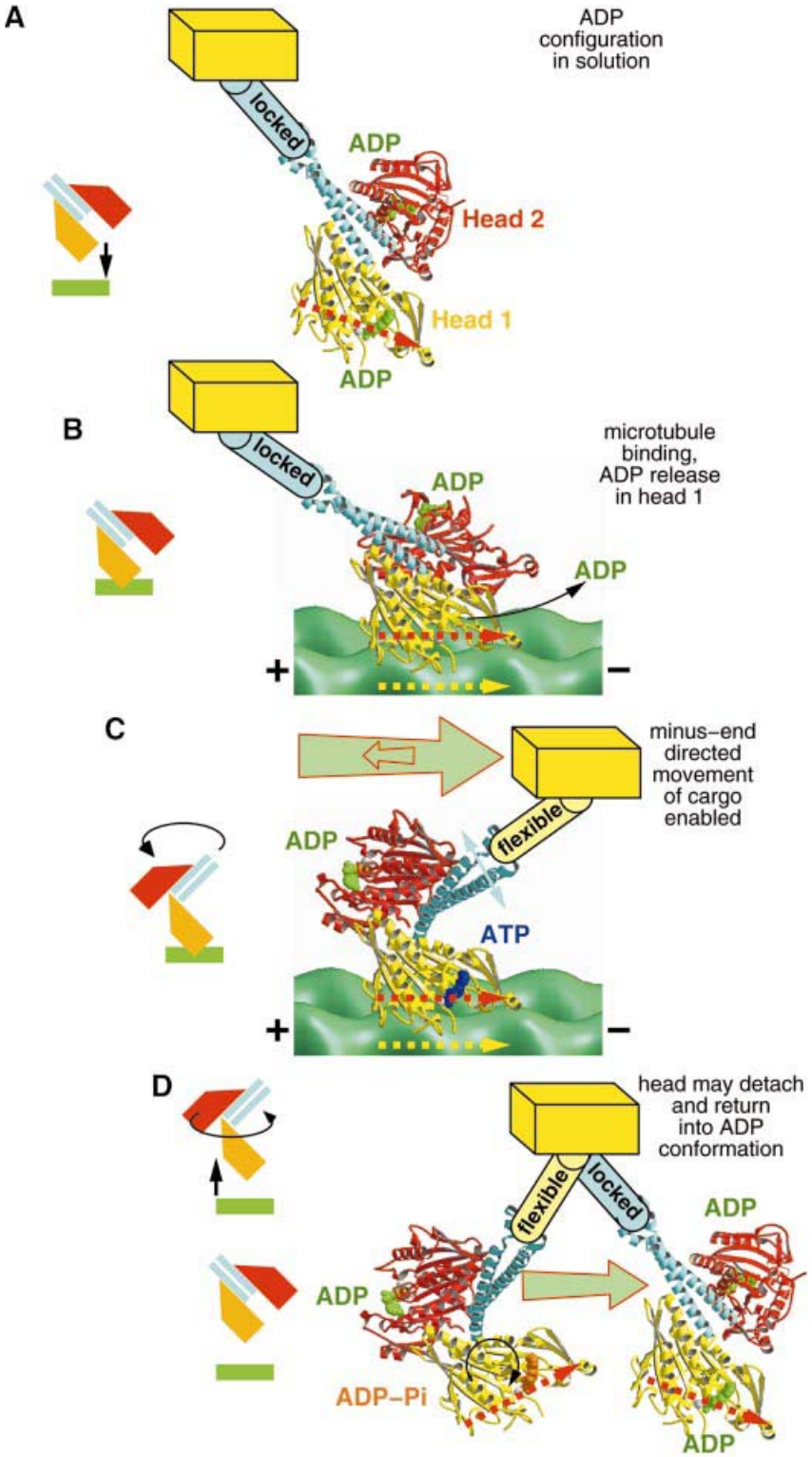

Fig. 5. Working model for the generation of a minus-end-directed power stroke by ncd based on our cryo-EM data combined with the X-ray structure of Sablin *et al*. (1998). (**A**) In solution, the ncd dimer has ADP bound and displays low affinity for tubulin. The neck–core interactions (see Figure 4) are intact and form a stable complex. To bind successfully to MTs, the head domain has to be directed into a position ahead of the cargo in the minus-end direction. To achieve a binding position, the yellow arrow (tubulin surface) and red arrow (motor domain) need to assume a parallel position. (**B**) Once in contact with the MT surface, head 1 (yellow) releases ADP, thereby increasing its binding affinity. Head 2 (red) maintains an ADP-bound state and does not make contact with the MT surface. (**C**) Head 1 binds ATP, which triggers a 90° rotation of head 2 including the entire coiled-coil neck around a radial axis going through the C-terminal end of the neck. Thereby, the neck–core interactions between head 1 and its helix α0 are released. (**D**) Once ATP is hydrolyzed, the ncd dimer could be released from the MT surface, and the dimer reforms the stable complex between neck and both cores.

significantly narrowing the gap between the two heads in the MT plus-end direction (Figure 3B). In the nucleotide-free state, this gap accommodates the neck, which now has to be relocated towards the MT minus end (Figures 3B and 4B). The only other alternative position would point its end directly into the lumen of the underlying MT, which is clearly not a reasonable solution. Most strikingly, the core–neck interactions in head 1 between the neck helices (α0) and helix α1 and loops 6, 10 and 13 have to be disrupted (Figure 4B). However, the extent of the interactions between head 2 and the neck is not clear at the achieved resolution of the reconstruction, but may remain conserved. In our modeled AMP-PNP dimer configuration, loops 6 and 10 of head 1 now come into close proximity to the region around loop 2, β1a/b and the beginning of α1 in head 2. However, the resolution here is not high enough to point out clearly any strong interactions between the heads in this modeled configuration. One potential interaction may occur between Lys568 and Gln569 on head 1 with Asp374 and Glu375 on head 2.

Possibly the entire complex, but in particular the coiled-coil neck region, appears to gain structural flexibility, indicated by the fact that the SH3 marker domains which we engineered to the ends of each neck helix are no longer visible. When using image reconstruction methods that rely on averaging over a large number of assumed identical images, the disappearance of some distinct structural elements such as the neck with its SH3 markers is a clear indication of a flexible position.

Discussion

Despite large structural similarities among the building plans of their motor head domains, conventional kinesin and ncd operate in very different ways. Conventional kinesin is a fast and highly processive anterograde motor which moves long distances without being released from the MT path. Several models exist which try to explain the mechanism involved in that processive motion. The most discussed ones are the so-called hand-over-hand model (Cross, 1999) and the more recently proposed inchworm model (Hua *et al*., 2002). Ncd, on the other hand, is significantly slower than kinesin, moves towards the minus end (McDonald and Goldstein, 1990) and is not processive (deCastro *et al*., 1999; Pechatnikova and Taylor, 1999; Foster and Gilbert, 2000). MTs are not only pathways for ncd, but also its main cargo. Ncd is involved in the organization of large assemblies (e.g. spindles) rather than transporting small cargos over long distances. Compared with kinesin, its dimeric motor domains exhibit very different conformations during its interaction with MTs. The strong MT-binding states of kinesin involve both heads simultaneously on two adjacent tubulin dimers (Hoenger *et al*., 2000). Ncd (in the absence of nucleotide or with AMP-PNP, mimicking the ATP state), however, binds to only one head at a time (Figure 2; Sosa *et al*., 1997; Hirose *et al*., 1998). Here we now introduce a mechanistic model for passive force transduction in ncd. We used cryo-EM and three-dimensional image reconstruction as the linking element between the physiological data available about ncd motor action (e.g. see McDonald and Goldstein, 1990; Foster and Gilbert, 2000; Foster *et al*., 2001) and the static atomic scale structural data derived from X-ray crystallography (Sablin *et al*., 1998).

A cooperative binding mechanism could help in forming polar microtubule organizations such as mitotic spindles

Our results obtained on MTs decorated with dimeric motor head domains at low stoichiometric ratios indicate that the binding process underlies a cooperative mechanism (Figure 1). Binding of an ncd motor molecule to the surface of MTs seems to increase the affinity for the next motor head along the same protofilament in the axial direction (Figure 1). Since the motor heads do not seem to touch each other in any direction, cooperative binding appears to be mediated via the tubulin portion. An interesting remaining question is how far such an induced conformational change might travel along a protofilament. This effect may be reminiscent of observed conformational changes induced in actin by actin-binding proteins (e.g. see McGough *et al*., 1997; Galkin *et al*., 2001). One could speculate that a cooperative mechanism enhances the bundling efficiency of ncd motors during their action in mitotic spindles by arranging MTs into oriented bundles and leading to an organization of the non-processive motors where they can work in conjunction, similarly to myosin II in the muscle lattice.

Ncd mediates minus-end-directed motion through regulation of its motor domain–neck interactions

Sablin *et al*. (1998) found that the ncd motor domains interact closely with their corresponding neck through various side chain interactions (see Figure 4A), and the functional relevance of these interactions has been analyzed by Endow and Higuchi (2000). Our data agree well with the conclusion that these interactions may play a crucial role in determining the preferred directionality of ncd towards the MT minus end. Here we found that ncd dimers, bound to MTs in a nucleotide-free state, still form a stable complex between head domains and its coiled-coil neck helices, similar to the configuration found in the ADP crystal structure (Figure 4A). As outlined in Figure 5, to assume an optimal orientation for MT binding, this stable head–neck conformation requires the motor domain to assume a position ahead of the attachment site on its cargo in the minus-end direction. In any other position, the geometry between the head and the MT surface would prevent the correct match of the motor-binding interface and the tubulin surface (see red arrows in head 1, Figure 5; Sablin, 2000). Successful binding can only occur when the head approaches the MT surface in an orientation that aligns the red arrow in head 1 with the yellow arrow on the tubulin surface, as illustrated in Figure 5B.

Similarly to the kinesin neck (Case *et al*., 1997; Henningsen and Schliwa, 1997; Rice *et al*., 1999), the ncd neck plays a crucial role in generating movement and determines directionality (see, for example, Endow and Higuchi, 2000). In kinesin, the catalytic core is connected to the α-helical coiled-coil neck via an elongated linker region (β9–β10; Kozielski *et al*., 1997). The corresponding neck linker region in ncd is an integrated part of the coiled-coil dimerization motif (Sablin *et al*., 1998) which exhibits typical coiled-coil-stabilizing heptad repeats and does not appear to melt easily; hence, a double binding

state as found for kinesin (Hoenger *et al*., 2000) seems less likely. However, in both cases, the density of the neck region is too low to be visualized directly by cryo-EM. Therefore, to enhance the neck's visibility, we labeled the N-terminal ends of the neck helices in our construct (Leu296) with globular SH3 domains directly engineered into the polypeptide chain. We have recently applied this strategy successfully to label the neck–linker region in monomeric and dimeric kinesin constructs (G.Skiniotis, T.Surrey, S.Altmann, H.Gron, Y.-H.Song, E.Mandelkow and A.Hoenger, submitted). The advantages over the commonly used gold labels are a 100% labeling efficiency and that there is no need to create cysteine-light mutants. Under structurally well-defined conditions, these labels allow for a high-resolution localization of distinct elements such as the end of the neck coiled-coil.

Three-dimensional reconstructions from MTs decorated with chimeric SH3–ncd dimers in the absence of nucleotides clearly revealed the SH3 domains, confirming that the stalk still points towards the MT plus end (Figures 2D, 3A and 4A). However, the helical three-dimensional reconstruction technique applied here relies on an averaging procedure over (presumably) identical image elements. Any flexible and floppy element will be lost during the reconstruction, somewhat similarly to areas with extreme temperature factors in crystallographic X-ray data. Therefore, unlike the situation for nucleotide-free conditions, we did not succeed in visualizing the ends of the neck coiled-coil in ncd–tubulin complexes in the presence of AMP-PNP, which is a clear indication of an increased flexibility of the neck region due to altered interactions causing conformational rearrangements within the dimeric complex (see Figures 2B, 3B and 4B).

ATP uptake causes a large conformational change within the MT-bound, dimeric ncd motor head complex. The rearrangement of head 1 and head 2 with respect to each other causes the interactions between head 1 (the bound one) and its neck to dissociate (Figure 4B). Thus, the heads approach each other with their regions around loops 6 and 10 in head 1 and loop 2, β1a/b and the beginning of α1 in head 2. This has two major effects: (i) it frees the neck and renders it more flexible (confirmed through the absence of SH3 labels in our reconstructions); and (ii) the gap between the two heads in the plus-end direction narrows and thereby forces the neck into a new position towards the minus end (Figures 4B and 5). The only other alternative would be a position that points directly into the MT lumen; however, this would not be compatible with a connection to cargo. At the same time, the core–neck interactions in head 2 could, in principle, remain intact (Figure 4B, dotted circles). Allowing for a slight flexibility of the neck–head 2 complex that would not average out the shape and orientation of head 2 in the reconstruction and also minor flexibility within the coiled-coil, we would expect to lose the signal for the SH3 domain located at this high radius. However, this is speculative and it may well be that all connections between neck and heads are broken.

In the model shown in Figure 5, we propose the cooperation of three key events to be responsible for an ncd action which directs cargo towards the minus end of MTs. (i) The stable interactions between ncd heads and its neck helices enforce an ncd–MT binding geometry which places the head domains ahead of the cargo in the minus-end direction. This binding geometry prevents a diffusion-controlled movement of the cargo in the plus-end direction once head 1 has bound to the MT (see also Sablin, 2000). At the same time, the intact head–neck interaction also prevents the cargo from moving in the minus-end direction until ATP binds to the MT-bound head. Ncd does not use its homodimeric head configuration for processivity, but for increasing the chance to bind to MTs with the right geometry. Ultimately, which head binds first is not important. (ii) ATP uptake dissociates the neck from the MT-bound head, which increases its flexibility. Now the cargo is free to move towards the minus end. Kinetic experiments have shown that head 2 does not release its ADP during that part of the cycle (deCastro *et al*., 2000; Foster *et al*., 2001). Therefore, it seems feasible to speculate that the neck–linker connections in head 2 remain intact, as suggested by our docking model which matches perfectly the cryo-EM three-dimensional scaffold (Figure 4B). (iii) The two heads rearrange in a way that closes the gap between loops 6 and 10 in head 1 and loop 2, β1a/b and the beginning of α1 in head 2, which is oriented in the plus-end direction. This might force the neck to relocate in the minus-end direction, and at the same time prevent backwards motion of the cargo. Motor action in ncd is most probaby not an active force applied to the cargo but more the formation of a barrier, preventing the cargo from moving backwards.

The cycle may then be completed with ATP hydrolysis, which will trigger the release of head 1 from the MT. This could close the cycle even without head 2 ever touching the MT surface. However, we cannot say from our data whether head 2 will go through a hydrolysis cycle as well immediately after head 1 has completed its cycle, or whether the motor is released from the MT surface and everything starts from the beginning (deCastro *et al*., 2000). Such a model is slightly incompatible with the results of Foster *et al*. (2001) where a double-binding state of ncd and a sequential ATP hydrolysis in both heads is proposed. However, the argument made by Foster *et al*. (2001) is based on an assumption that could be controversial in our view, and our structural data and those from X-ray crystallography (Sablin *et al*., 1998) argue against (but do not exclude) the possibility of a double-binding conformation. The only way to achieve a double-binding conformation in ncd would be by partially melting the (rather stable) neck coiled-coil; otherwise two adjacent binding sites cannot be reached simultaneously as there are steric constraints. We have shown here that, unlike the case for kinesin, the strong MT-binding states of dimeric ncd are clearly asymmetric. MT binding is only achieved through one head while holding both heads in close proximity. Accordingly, there is no structural evidence so far for a potential double-binding configuration of dimeric ncd, either from X-ray crystallography or from EM three-dimensional reconstructions (Sosa *et al*., 1997; Hirose *et al*., 1998; this work).

The swing of the neck that we propose from our data agrees well with the purely hypothetical model as proposed for ncd previously (see Figure 2C; Kikkawa *et al*., 2001). This model was based on the nucleotide-dependent movement of the neck linker due to reorganization of the switch II cluster in the monomeric kinesin motor KIF1A. The mechanistic model proposed here

would not suit any fast and processive motor action, but makes perfect sense for a non-processive motor involved in a task such as mitotic spindle formation and the organization of large complex assemblies in a cell. The mechanism proposed here slightly resembles the action of myosin II in muscle, but without the benefit of a sophisticated force-generating apparatus as found in myosin heads. A motor like ncd, which acts together in large groups on large cargos, does not require a processive mechanism to be kept on track. The high degree of bundling activity, observed for wild-type ncd and any dimeric construct, agrees well with its biological function in organizing MTs. The ncd heads are automatically kept close to their path by the complexity of the entire system with which it is involved. The two heads of an ncd dimer are used, not for an alternating and processive motion in the way that conventional kinesin works, but to increase the chance of binding to the road in a suitable geometry, and to generate the minus-end-directed motion through the conformational changes proposed here.

Materials and methods

Expression and purification of dimeric ncd motor domains

Plasmid pNcd296, coding for the 404 C-terminal amino acids of ncd (residues 296–700) was cloned by insertion of two oligo pairs into a vector pNcd343 coding for a monomeric ncd construct (E.Mandelkow, unpublished; derived using a construct GST–N300, which was a gift from L.S.B.Goldstein, as a template). The 62 codon spectrin SH3 in a pBAT4 plasmid (a kind gift from L.Serrano) was PCR amplified. The SH3–ncd296 construct was cloned by insertion of the spectrin SH3 sequence into the N-terminal end of the ncd sequence.

The dimeric ncd protein, representing residues 296–700 of ncd and the SH3–ncd296 chimera, was expressed in *Escherichia coli* BL21 (DE3) by induction with 0.2 mM isopropyl-β-D-thiogalactopyranoside (IPTG) for 16 h at 24°C. Cells were resuspended in lysis buffer [50 mM PIPES pH 6.9, 1 mM EGTA, 1 mM $MgCl_2$, 1 mM dithiothreitol (DTT), 1 mM phenylmethylsulfonyl fluoride (PMSF), 50 mM NaCl, 100 μM MgATP], and lysed using a French press (Aminco, Urbana, IL). The protein was purified with two ion exchange columns (phosphocellulose and SP-Sepharose or MonoS). Finally, the protein was dialyzed against 20 mM PIPES pH 6.9, 1 mM EGTA, 1 mM DTT, 1 mM $MgCl_2$ and 100 mM NaCl, and concentrated using an Ultrafree 30 concentrator (Millipore).

Decoration of microtubules with ncd

Tubulin was purchased from Cytoskeleton Inc. (Denver, CO). MTs were polymerized for 20 min at 37°C in 80 mM PIPES pH 6.8, 2 mM $MgCl_2$, at a concentration of 5 mg/ml and in the presence of 10% (v/v) dimethylsulfoxide (DMSO), 2 mM GTP and 20 μM taxol. Decoration of polymerized MTs with dimeric ncd constructs was performed in solution at a final tubulin concentration of 0.5 mg/ml (~5 μM αβ-tubulin heterodimers) and varying ncd concentration from 0.21 to 4.5 mg/ml (~2.3–55 μM). The SH3–ncd construct was mixed with the tubulin solution at a concentration of 4.4 mg/ml (~42 μM). Thus the stoichiometry of ncd heads to tubulin heterodimers ranged from 0.5 to 12, and that of the SH3–ncd construct was 9:1. Experiments were done either in the presence of 2 mM AMP-PNP, 2 mM MgADP or after incubation with apyrase. Samples were incubated for 2 min and subsequently adsorbed to holey carbon grids for 1 min and quick-frozen in liquid ethane by using a plunger, essentially following the standard procedures described by Dubochet *et al*. (1988). In some experiments, decoration of MTs was performed directly on the grid to avoid bundling of tubules. In these cases, MTs at a concentration of 1 mg/ml were adsorbed on holey carbon grids for 1 min, incubated for 2 min with an ncd solution at varying concentrations and quick-frozen as described above.

Cryo-electron microscopy, image processing and three-dimensional reconstruction

Cryo-EM was performed on a Philips CM20 and a CM200-FEG microscope, using a GATAN-626 cryo-holder. Images were recorded at 38 000× magnification on Kodak SO-163 EM film at a defocus of –1.5 to –2.0 μm.

For three-dimensional reconstructions, we screened images for 15 protofilament/2 start helical MTs (see Beuron and Hoenger, 2001). Micrographs were digitized using a Zeiss-SCAI scanner at a step size of 21 μm corresponding to 0.553 nm on the original object. Suitable MTs were reconstructed helically by using the program suite PHOELIX (Whittaker *et al*., 1995). All data sets were truncated to a maximum resolution of 25 Å. Three-dimensional maps were visualized by using SUPRIM (Schroeter and Bretaudiere, 1996) and AVS (Advanced Visualization Software).

Molecular docking and modeling

In order to interpret the three-dimensional reconstructions at near atomic detail, we docked components of the dimeric ncd crystal structure (Sablin *et al*., 1998) (PDB ID code 2NCD.pdb), the high-resolution structure of the αβ-tubulin dimer (Nogales *et al*., 1998) (PDB ID code 1TUB.pdb) and the spectrin SH3 domain (PDB ID code 1BKZ.pdb; Martinez *et al*., 1998) into the EM electron density map. Interactive docking was performed using the modeling program 'O' (Jones *et al*., 1991) as well as the program suite COAN (Volkmann and Hanein, 1999). COAN is based on a global evaluation of real-space correlation and the identification of sets of solutions that fit the experimental three-dimensional reconstructions at a chosen confidence level equally well (Volkmann *et al*., 2000). We used a confidence level of 99.9% ($P = 0.001$) throughout this study. We used four independent rigid bodies to perform the docking in a modular fashion. (i) The tubulin protofilament (Nogales *et al*., 1998) was fitted to each of the three-dimensional reconstructions. This docking resulted in a well-defined solution set, consistent with previous docking studies (Nogales *et al*., 1999). (ii) Discrepancy maps that removed the contribution of the fitted protofilaments from the three-dimensional reconstructions were generated as described previously (Volkmann and Hanein, 1999). The coordinates of single ncd heads were fitted into these discrepancy maps. This docking head led to a solution set that consists of three separate subsets. There is no significant difference between these three solutions at the 99.9% confidence level. However, two of the subsets are incompatible with the available biochemical and mutagenesis data (Woehlke *et al*., 1997; Alonso *et al*., 1998). The third set is consistent with our previous interactive docking of the monomeric ncd motor domain into an EM-derived three-dimensional envelope (Hoenger *et al*., 1998). In combination with the protofilament docking, this orientation identified the region of helix 12 in β-tubulin as one of the major contact zones (figure 7 in Nogales *et al*., 1999). (iii) A second set of discrepancy maps was calculated by removing the contributions of the fitted single ncd heads and protofilaments from the three-dimensional reconstructions. This map shows patches of density close to the MT surface, indicating that the three-dimensional reconstruction in this region cannot be explained by the addition of the ncd head to the fitted protofilament model alone. Changes in conformation and/or stability at the MT surface are also likely to take place. Single ncd heads (corresponding to the second monomer) were fitted into the portion of the AMP-PNP discrepancy map distal from the MT. This docking resulted in one single, well-defined solution set, indicating that the orientation of the head is well defined and the three-dimensional reconstruction can be described sufficiently well by the addition of the second head in this region. (iv) The position of the neck was modeled based on the position of the neck helix in the second head after docking using the X-ray crystallography modeling program O (Jones *et al*., 1991). Figures of the model were prepared using Bobscript 2.3 (Esnouf, 1997).

Acknowledgements

This work was in part supported by a grant from NIH (GM64473) to N.V. and by a grant from the DFG HO2276/1-1.

References

Alonso,M., Damme,J., Vandekerkhove,J. and Cross,R.A. (1998) Proteolytic mapping of kinesin/ncd-microtubule interface: nucleotide-dependent conformational changes in the loops L8 and L12. *EMBO J.*, **17**, 945–951.

Beuron,F. and Hoenger,A. (2001) Structural analysis of the microtubule–kinesin complex by cryo-electron microscopy. In Vernos,I. (ed.), *Methods in Molecular Biology*. Humana Press, Totowa, NJ, pp. 235–254.

Bloom,G.S. and Goldstein,L.S. (1998) Cruising along microtubule

highways: how membranes move through the secretory pathway. *J. Cell Biol.*, **140**, 1277–1280.
Case,R.B., Pierce,D.W., Hom-Booher,N., Hart,C.L. and Vale,R.D. (1997) The directional preference of kinesin motors is specified by an element outside of the motor catalytic domain. *Cell*, **90**, 959–966.
Chandra,R., Salmon,E.D., Erickson,H.P., Lockhart,A. and Endow,S.A. (1993) Structural and functional domains of the *Drosophila* ncd microtubule motor protein. *J. Biol. Chem.*, **268**, 9005–9013.
Cross,R.A. (1999) Molecular motors: walking talking heads. *Curr. Biol.*, **9**, R854–R856.
deCastro,M.J., Ho,C.H. and Stewart,R.J. (1999) Motility of dimeric ncd on a metal-chelating surfactant: evidence that ncd is not processive. *Biochemistry*, **38**, 5076–5081.
deCastro,M.J., Fondecave,R.M., Clarke,L.A., Schmidt,C.F. and Stewart,R.J. (2000) Working strokes by single molecules of the kinesin-related microtubule motor ncd. *Nat. Cell Biol.*, **2**, 724–729.
Dubochet,J., Adrian,M., Chang,J.J., Homo,J.C., Lepault,J., McDowall,A.W. and Schultz,P. (1988) Cryo-electron microscopy of vitrified specimens. *Q. Rev. Biophys.*, **21**, 129–228.
Endow,S.A. and Higuchi,H. (2000) A mutant of the motor protein kinesin that moves in both directions on microtubules. *Nature*, **406**, 913–916.
Esnouf,R.M. (1997) An extensively modified version of MolScript that includes greatly enhanced coloring capabilities. *J. Mol. Graph. Model.*, **15**, 132–134.
Foster,K.A. and Gilbert,S.P. (2000) Kinetic studies of dimeric ncd: evidence that ncd is not processive. *Biochemistry*, **39**, 1784–1791.
Foster,K.A., Correia,J.J. and Gilbert,S.P. (1998) Equilibrium binding studies of non-claret disjunctional protein (ncd) reveal cooperative interactions between the motor domains. *J. Biol. Chem.*, **273**, 35307–35318.
Foster,K.A., Mackey,A.T. and Gilbert,S.P. (2001) A mechanistic model for ncd directionality. *J. Biol. Chem.*, **276**, 19259–19266.
Galkin,V.E., Orlova,A., Lukoyanova,N., Wriggers,W. and Egelman,E.H. (2001) Actin depolymerizing factor stabilizes an existing state of F-actin and can change the tilt of F-actin subunits. *J. Cell Biol.*, **153**, 75–86.
Geeves,M.A. and Holmes,K.C. (1999) Structural mechanism of muscle contraction. *Annu. Rev. Biochem.*, **68**, 687–728.
Henningsen,U. and Schliwa,M. (1997) Reversal in the direction of movement of a molecular motor. *Nature*, **389**, 93–96.
Hirokawa,N. (1998) Kinesin and dynein superfamily proteins and the mechanism of organelle transport. *Science*, **279**, 519–526.
Hirose,K., Lockhart,A., Cross,R.A. and Amos,L.A. (1996) Three-dimensional cryoelectron microscopy of dimeric kinesin and ncd motor domains on microtubules. *Proc. Natl Acad. Sci. USA*, **93**, 9539–9544.
Hirose,K., Cross,R.A. and Amos,L.A. (1998) Nucleotide-dependent structural changes in dimeric NCD molecules complexed to microtubules. *J. Mol. Biol.*, **278**, 389–400.
Hoenger,A. and Milligan,R.A. (1997) Motor domains of kinesin and ncd interact with microtubule protofilaments with the same binding geometry. *J. Mol. Biol.*, **265**, 553–564.
Hoenger,A., Sack,S., Thormählen,M., Marx,A., Muller,J., Gross,H. and Mandelkow,E. (1998) Image reconstructions of microtubules decorated with monomeric and dimeric kinesins: comparison with X-ray structure and implications for motility. *J. Cell Biol.*, **141**, 419–430.
Hoenger,A., Thormählen,M., Diaz-Avalos,R., Doerhoefer,M., Goldie, K.N., Muller,J. and Mandelkow,E. (2000) A new look at the microtubule binding patterns of dimeric kinesins. *J. Mol. Biol.*, **297**, 1087–1103.
Hua,W., Chung,J. and Gelles,J. (2002) Distinguishing inchworm and hand-over-hand processive kinesin movement by neck rotation measurements. *Science*, **295**, 844–848.
Jones,T.A., Zou,J.-Y., Cowan,W. and Kjeldgaard,M. (1991) Improved methods for building protein models in electron density maps and the location of errors in these models. *Acta Crystallogr. A*, **47**, 110–119.
Kikkawa,M., Sablin,E.P., Okada,Y., Yajima,H., Fletterick,R.J. and Hirokawa,N. (2001) Switch-based mechanism of kinesin motors. *Nature*, **411**, 439–445.
Kozielski,F., Sack,S., Marx,A., Thormählen,M., Schönbrunn,E., Biou,V., Thompson,A., Mandelkow,E.-M. and Mandelkow,E. (1997) The crystal structure of dimeric kinesin and implications for microtubule-dependent motility. *Cell*, **91**, 985–994.
Lanzetta,P.A., Alvarez,L.J., Reinach,P.S. and Candia,O.A. (1979) An improved assay for nanomole amounts of inorganic phosphate. *Anal. Biochem.*, **100**, 95–97.
Mandelkow,E. and Johnson,K.A. (1998) The structural and mechano-chemical cycle of kinesin. *Trends Biochem. Sci.*, **23**, 429–433.
Mandelkow,E. and Hoenger,A. (1999) Structures of kinesin and kinesin–microtubule interactions. *Curr. Opin. Cell Biol.*, **11**, 34–44.
Martinez,J.C., Pisabarro,M.T. and Serrano,L. (1998) Obligatory steps in protein folding and the conformational diversity of the transition state. *Nat. Struct. Biol.*, **5**, 721–729.
McDonald,H.B. and Goldstein,L.S. (1990) Identification and characterization of a gene encoding a kinesin-like protein in *Drosophila*. *Cell*, **61**, 991–1000.
McDonald,H.B., Stewart,R.J. and Goldstein,L.S. (1990) The kinesin-like ncd protein of *Drosophila* is a minus end-directed microtubule motor. *Cell*, **63**, 1159–1165.
McGough,A., Pope,B., Chiu,W. and Weeds,A. (1997) Cofilin changes the twist of F-actin: implications for actin filament dynamics and cellular function. *J. Cell Biol.*, **138**, 771–781.
Nogales,E., Wolf,S. and Downing,K. (1998) Structure of the αβ tubulin dimer by electron crystallography. *Nature*, **391**, 199–203.
Nogales,E., Whittaker,M., Milligan,R.A. and Downing,K.H. (1999) High-resolution model of the microtubule. *Cell*, **96**, 79–88.
Pechatnikova,E. and Taylor,E.W. (1999) Kinetics processivity and the direction of motion of ncd. *Biophys. J.*, **77**, 1003–1016.
Rice,S. *et al*. (1999) A structural change in the kinesin motor protein that drives motility. *Nature*, **402**, 778–784.
Sablin,E.P. (2000) Kinesins and microtubules: their structures and motor mechanisms. *Curr. Opin. Cell Biol.*, **12**, 35–41.
Sablin,E.P., Kull,F.J., Cooke,R., Vale,R.D. and Fletterick,R.J. (1996) Crystal structure of the motor domain of the kinesin-related motor ncd. *Nature*, **380**, 555–559.
Sablin,E.P., Case,R.B., Dai,S.C., Hart,C.L., Ruby,A., Vale,R.D. and Fletterick,R.J. (1998) Direction determination in the minus-end-directed kinesin motor ncd. *Nature*, **395**, 813–816.
Schroeter,J.P. and Bretaudiere,J.P. (1996) SUPRIM: easily modified image processing software. *J. Struct. Biol.*, **116**, 131–137.
Sheetz,M.P. (1999) Motor and cargo interactions. *Eur. J. Biochem.*, **262**, 19–25.
Sosa,H., Dias,D.P., Hoenger,A., Whittaker,M., Wilson-Kubalek,E., Sablin,E., Fletterick,R.J., Vale,R.D. and Milligan,R.A. (1997) A model for the microtubule–ncd motor protein complex obtained by cryo-electron microscopy and image analysis. *Cell*, **90**, 217–224.
Vale,R.D. and Milligan,R.A. (2000) The way things move: looking under the hood of molecular motor proteins. *Science*, **288**, 88–95.
Vilfan,A., Frey,E., Schwabl,F., Thormahlen,M., Song,Y.H. and Mandelkow,E. (2001) Dynamics and cooperativity of microtubule decoration by the motor protein kinesin. *J. Mol. Biol.*, **312**, 1011–1026.
Volkmann,N. and Hanein,D. (1999) Quantitative fitting of atomic models into observed densities derived by electron microscopy. *J. Struct. Biol.*, **125**, 176–184.
Volkmann,N., Hanein,D., Ouyang,G., Trybus,K.M., DeRosier,D.J. and Lowey,S. (2000) Evidence for cleft closure in actomyosin upon ADP release. *Nat. Struct. Biol.*, **7**, 1147–1155.
Walker,R.A., Salmon,E.D. and Endow,S.A. (1990) The *Drosophila* claret segregation protein is a minus-end directed motor molecule. *Nature*, **347**, 780–782.
Whittaker,M., Carragher,B.O. and Milligan,R.A. (1995) PHOELIX: a package for semi-automated helical reconstruction. *Ultramicroscopy*, **58**, 245–259.
Woehlke,G., Ruby,A.K., Hart,C.L., Ly,B., Hom-Booher,N. and Vale,R.D. (1997) Microtubule interaction site of the kinesin motor. *Cell*, **90**, 207–216.

Received July 3, 2002; revised September 23, 2002; accepted September 30, 2002